

Article

A Study of the Optical and Structural Properties of SnO₂ Nanoparticles Synthesized with *Tilia cordata* Applied in Methylene Blue Degradation

Eduardo Quintero González ¹, Eder Lugo Medina ^{2,*}, Reina Vianey Quevedo Robles ¹,
Horacio Edgardo Garrafa Gálvez ³, Yolanda Angelica Baez Lopez ¹, Eunice Vargas Viveros ¹,
Ferdinandina Aguilera Molina ¹, Alfredo Rafael Vilchis Nestor ⁴ and Priscy Alfredo Luque Morales ^{1,*}

¹ Facultad de Ingeniería, Arquitectura y Diseño-Universidad Autónoma de Baja California, Ensenada C.P. 22860, Baja California, Mexico

² Tecnológico Nacional de México-IT de Los Mochis, Los Mochis C.P. 81259, Sinaloa, Mexico

³ Departamento de Ingeniería y Tecnología, Universidad Autónoma de Occidente (UadeO), Guasave C.P. 81048, Sinaloa, Mexico

⁴ Centro Conjunto de Investigación en Química Sustentable, UAEM-UNAM, Toluca C.P. 50200, Mexico

* Correspondence: eder.lm@mochis.tecnm.mx (E.L.M.); pluque@uabc.edu.mx (P.A.L.M.)

Citation: González Quintero, E.; Lugo Medina, E.; Quevedo Robles, R.V.; Garrafa Gálvez, H.E.; Baez Lopez, Y.A.; Vargas Viveros, E.; Aguilera Molina, F.; Vilchis Nestor, A.R.; Luque Morales, P.A. A Study of the Optical and Structural Properties of SnO₂ Nanoparticles Synthesized with *Tilia cordata* Applied in Methylene Blue Degradation. *Symmetry* **2022**, *14*, 2231. <https://doi.org/10.3390/sym14112231>

Academic Editors: Sergei D. Odintsov and György Keglevich

Received: 16 September 2022

Accepted: 18 October 2022

Published: 24 October 2022

Publisher's Note: MDPI stays neutral with regard to jurisdictional claims in published maps and institutional affiliations.



Copyright: © 2022 by the authors. Licensee MDPI, Basel, Switzerland. This article is an open access article distributed under the terms and conditions of the Creative Commons Attribution (CC BY) license (<http://creativecommons.org/licenses/by/4.0/>).

Abstract: Water contamination is one of the most worrisome problems in the world. Industrial dyes are discharged without previous treatment, promoting water pollution and affecting the environment. In this paper, semiconductor SnO₂ nanoparticles (NPs) were synthesized using *Tilia cordata* extract, as a reducing agent, at different concentrations, 1%, 2%, and 4% (weight/volume; *w/v*). These NPs were used as photocatalysts characterize an alternative for degrading wastewater compounds. Nanoparticle symmetry is an important factor for understanding the properties that provide tools for further treatments. Additionally, the structural, morphological, and optical properties of the green-synthesized SnO₂ NPs were studied. Fourier transform infrared spectroscopy (FTIR) showed the characteristic absorption band of Sn–O centered at 609 cm⁻¹. Meanwhile, X-ray diffraction (XRD) confirmed a tetragonal rutile-type crystalline phase without impurities whose crystallite size increased from 15.96 nm and 16.38 nm to 21.51 nm for SnO₂-1%, SnO₂-2%, and SnO₂-4%, respectively, as extract concentration was increased. NPs with a quasi-spherical morphology with agglomerations were observed through scanning electron microscopy (SEM). On the other hand, the bandgap remained at ~3.6 eV throughout all samples, even at variable extract concentrations. The NPs yielded great photocatalytic activity capable of degrading methylene blue (MB) dye under ultraviolet radiation and solar radiation, achieving degradation percentages of 90% and 83% of MB under UV and solar radiation at 90 and 180 min, respectively.

Keywords: SnO₂; *Tilia cordata*; photocatalysis; methylene blue

1. Introduction

Water pollution is one of the major problems worldwide, caused by industrial waste discharge such as organic dyes, which are considered pollutants in concentrations from 1 ppm [1]. Due to their chemical structure, dyes are resistant to solar radiation and to the action microorganisms [2], which makes them slow-degrading and nonbiodegradable contaminants. In humans, they are considered mutagenic and can cause malnutrition as a result of bioaccumulation. In addition, they cause skin and eye irritation, kidney, and respiratory problems [3–6]. Furthermore, dyes prevent reoxygenation and sunlight passage through bodies of water, causing adverse effects on aquatic life [7]. Throughout history, different physical or chemical methods have been developed to remove dyes, for instance, adsorption [8], coagulation–flocculation [9], ozonation [10], and biological

methods [11], among others. These procedures are considered highly efficient; however, they require additional treatment since they generate byproducts, and even worse, some use toxic chemical agents. Alternatively, photocatalysis, reported in 1987 by Fujishima and Honda [12], has positioned itself as one of the most promising advanced oxidation chemical methods today [13] due to its ability to degrade organic dyes until their mineralization and to its working conditions, atmospheric temperature, and pressure and under solar or UV radiation [14]. SnO₂ being photoexcited by irradiating it with an energy equal to its bandgap or greater, generating electron-hole pairs that interact with H₂O and O₂ molecules in the solution, giving rise to reactive species that act on the dye degrading it [15]. Semiconductor oxide nanoparticles, such as TiO₂ [16], ZnO [17], Co/Co₃O₄ [18], Nb₂O₅ [19], BiVO₄ [20], DyBa₂Fe₃O_{7.988}/DyFeO₃ [21] and SnO₂ [22], whose high surface area allows greater interaction with dyes, have been widely used in photocatalysis. SnO₂ has stood out for its high stability, high oxidation potential, corrosion resistance, and nontoxicity, as well as for its excellent photocatalytic activity [23]. Within the NPs, SnO₂ semiconductor synthesis methods excel on the basis of using natural precursors like extracts from plants [24–26], algae [27], fungi [28], and bacteria [29] that contain primary metabolites and secondary polyphenols such as flavonoids and terpenes, which can reduce metal salts to metal ion NPs. In addition, they can stabilize NPs by avoiding contact between nuclei, preventing fusion and hence controlling their size. Using natural extracts decreases the inherent environmental impacts of chemical processes, making them safe, biocompatible, and eco-friendly [30]. Diverse research on SnO₂ NP green synthesis using plant extracts has been reported in the literature. Suresh et al. [31] used *Delonix elata* for synthesizing NPs between 13 and 19 nm whose photocatalytic activity in the rhodamine B degradation was evaluated, rendering a maximum degradation of 92.8% after 150 min under UV radiation. Karthik et al. [32] obtained SnO₂ NPs through microwave-assisted green synthesis using *Andrographis paniculata* extracts; the NPs were evaluated for their optical and photocatalytic properties in Congo red dye degradation. Rathinabala et al. [33] used *Canna indica* leaf extracts obtaining SnO₂ NPs that were analyzed for rhodamine B degradation under UV and sun radiation; cytotoxicity was also evaluated. To the best of our knowledge, there are no reports within the literature on SnO₂ NPs biosynthesized utilizing *Tilia cordata* extracts. *Tilia cordata*, also known as lime or linden, is a straight-stemmed tree with a smooth bark that can reach 18 m in height. Its leaves are heart-shaped, dark green on the upper side, and bluish green on the underside. Its flowers are yellowish in color, grouped in clusters of one to six flowers that mature into globose-looking fruits [34]. At least 24 water-soluble phenolic compounds have been detected in its extract with a flavonoids and antioxidants high content, in a 58.86 ± 21.51 y 82.99 ± 13.13 mg/g proportion, respectively [35]. These molecules can be used in NP semiconductor green synthesis. In the present work, semiconductor SnO₂ NPs were synthesized through biosynthesis utilizing *Tilia cordata* extracts at different concentrations to evaluate their photocatalytic activity in MB degradation.

2. Materials and Methods

2.1. Materials

Stems, leaves, and flowers of *Tilia cordata* were obtained at a local market. Tin chloride (SnCl₂•2H₂O, 98%), used as tin precursor salt, and Methylene blue, as model dye, were purchased at Sigma-Aldrich. Deionized water was used as environmentally friendly solvent. All reagents were used as received.

2.2. *Tilia Cordata* Extract Preparation

Tilia cordata extract was prepared using a thermal method in an aqueous solution. Briefly, to prepare *Tilia cordata* extract, the stems, leaves, and flowers were pulverized. Subsequently, 1%, 2%, and 4% (*w/v*) extract solutions were prepared in 50 mL deionized water. The solutions remained under magnetic stirring for 2 h. They were consecutively

placed in a water bath at 60 °C for 1 h. Afterward, the extracts were vacuum filtered to separate them from the organic matter. The extracts were stored for further use.

2.3. Green Synthesis of SnO₂ NPs

In a typical procedure: 2 g of SnCl₂•2H₂O were dissolved in 42 mL of the *Tilia cordata* extract, 1%, 2%, and 4% (*w/v*), labeled SnO₂-1%, SnO₂-2%, and SnO₂-4%, respectively. The solutions were mechanically stirred for 1 h until the Sn precursor's complete dissolution, then placed in a thermoregulated water bath at 60 °C for 12 h to complete the reaction until a pasty consistency was obtained. Finally, they were submitted to heat treatment at 400 °C for 1 h. The grayish-white products were ground and stored for later characterization and photocatalytic activity evaluation.

2.4. Characterization Techniques of the NPs

The SnO₂-1%, SnO₂-2%, and SnO₂-4% NPs were characterized by different analytical techniques. The functional groups were analyzed by Fourier transform infrared spectroscopy (FTIR) with attenuated total reflectance (ATR), using a Perkin Elmer Spectrum Two Spectrophotometer; the spectra were taken in a 4500 cm⁻¹ to 300 cm⁻¹ range. The XRD diffraction patterns were obtained in a Bruker X-ray D2 phase diffractometer with a 1.5406 Å (Cu Kα) irradiation wavelength. The scanning angle was measured in a 10° to 80° range at a 0.02° step. Morphology was determined utilizing a JEOL JSM-6310LV scanning electron microscope (SEM) operating at 200 kV. Sample purity was probed by elemental composition analysis using energy-dispersive X-ray spectroscopy (EDX). The optical properties analyses were carried out by visible-ultraviolet light (UV-Vis) and photoluminescence (PL) spectroscopies. The UV-Vis analysis was performed in a Perkin Elmer Lambda 365 equipment at a 600 nm/min scanning speed, in the 200 nm to 800 nm wavelength range. The PL analysis was performed on a Horiba Nanolog PL spectrophotometer over a 200 nm to 600 nm wavelength range and 350 nm excitation wavelength.

2.5. Photocatalytic Activity

The SnO₂ NPs photocatalytic activity was evaluated for MB dye degradation at a 15 ppm concentration. Degradation studies were performed using UV and solar radiation. In the experiment under UV radiation, 10 W Polaris UV-1C lamps with an energy of 18 mJ/cm² were used. In a typical experiment, 50 mg of SnO₂-1%, SnO₂-2%, and SnO₂-4% NPs were added to 50 mL of MB dye solution. The obtained suspension was then mechanically shaken in the dark for 30 min to obtain the adsorption–desorption equilibrium. Subsequently, the suspensions were placed under UV radiation. During the experiment, aliquots were taken at progressive times for up to 180 min. Analogously, the experiment carried out under solar radiation followed a procedure similar to that described above. MB photodegradation was studied from 10:00 am to 1:00 pm on sunny days during October in Ensenada, Baja California, Mexico. The degraded samples' absorbance measurements were provided by UV-Vis spectroscopy. Degradation calculations were performed according to Equation (1):

$$\eta = 1 - (C_t/C_0) \quad (1)$$

where η is degradation efficiency, C_t is dye concentration at any given time, and C_0 is the initial dye concentration.

3. Results and Discussion

3.1. Fourier Transform Infrared Spectroscopy Analysis

Figure 1 shows the FTIR spectra in ATR mode for the *Tilia cordata* extract and the SnO₂-1%, SnO₂-2%, and SnO₂-4% NPs. The *Tilia cordata* spectrum in Figure 1a shows an absorption band centered at 3323 cm⁻¹ that is attributed to the vibrations of the O–H bond; the signals located at 2925 and 2851 cm⁻¹ can be attributed to the C–H bond vibrations of

methyls and methylenes, respectively, whereas the absorption bands centered at 1731–1600 cm^{-1} are attributed to the C=O bond vibrational mode [36]. The SnO_2 NPs with 1%, 2%, and 4% extract (Figure 1a,b) presented 2 characteristic signals centered at 605 and 480 cm^{-1} , which are attributed to the asymmetric and symmetric Sn–O and Sn–O–Sn stretching, respectively [37,38]. Additionally, it is possible to observe the absorption bands corresponding to *Tilia cordata* located at 3400 cm^{-1} , 2925 cm^{-1} , 2851 cm^{-1} , and 1636 cm^{-1} , indicating the presence of extract molecules in the SnO_2 synthesized products [39,40].

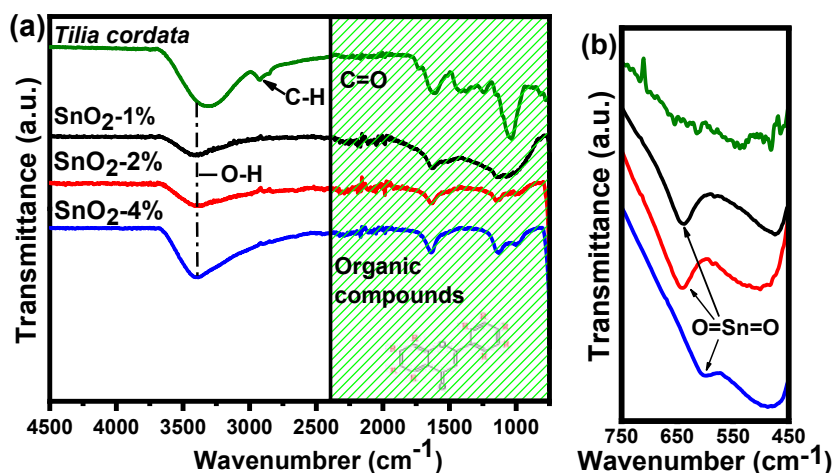


Figure 1. FTIR-ATR spectra of (a) *Tilia cordata* extract and SnO_2 -1%, SnO_2 -2%, and SnO_2 -4% NPs and (b) insert: infrared region from 750 cm^{-1} to 450 cm^{-1} .

3.2. X-ray Diffraction

The XRD patterns of the SnO_2 -1%, SnO_2 -2%, and SnO_2 -4% NPs are shown in Figure 2. The diffractograms display several well-defined peaks located at 26.53°, 33.82°, 37.95°, 51.75°, 54.5°, 57.85°, 61.88°, 64.75°, and 65.9° 2θ that correspond to planes (110), (101), (200), (211), (220), (002), (310), (112), and (301), respectively. The crystallographic planes are assigned to the SnO_2 , tetragonal rutile crystal phase, according to the crystallographic chart No.41-1445 from JCPDS database, confirming crystalline SnO_2 achieved using 1%, 2%, and 4% (*w/v*) *Tilia cordata* extract [41,42]. Additionally, the absence of other peaks indicates only one phase without impurities.

The SnO_2 NPs crystallite size was determined using the Debye–Scherrer model, Equation (2).

$$\tau = (K\lambda) / (\beta \cos \theta) \quad (2)$$

where τ is the average crystallite size, K is the dimensionless shape factor at ~ 0.9 , λ is the X-ray wavelength, β is the full width at half maximum intensity (FWHM), and θ is the Bragg angle. According to Equation (2), the crystallite sizes of the SnO_2 -1%, SnO_2 -2%, and SnO_2 -4% synthesized NPs are 15.96 nm, 16.38 nm, and 21.51 nm, respectively, indicating an increase in crystallite size as extract concentration increases, denoting that the use of *Tilia cordata* extract facilitates SnO_2 crystal growth [43].

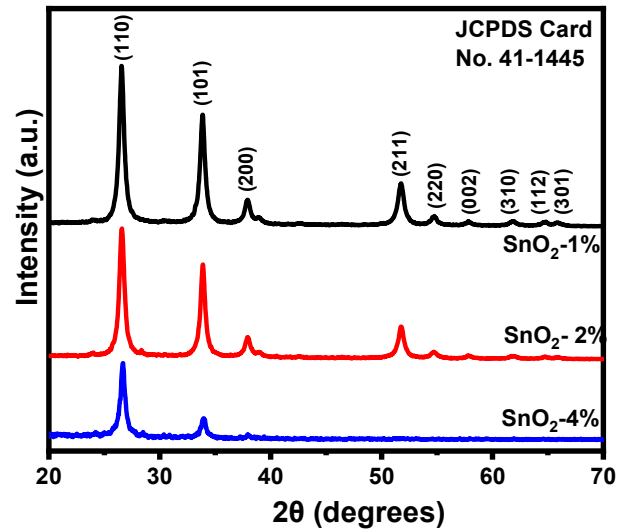


Figure 2. XRD patterns of SnO₂ NPs synthesized with different concentrations of *Tilia cordata* extract.

3.3. Optical Properties

Figure 3 illustrates the UV-Vis absorption spectra of the SnO₂-1%, SnO₂-2%, and SnO₂-4% NPs. In all the syntheses, an absorption edge centered ~300 nm was detected, which is characteristic of SnO₂ semiconductors according to reports in the literature [44,45]. Bandgap calculation was performed using the Tauc model, Equation (3): [46]

$$\alpha(\nu)h\nu = K(h\nu - E_g)^n \quad (3)$$

where E_g corresponds to bandgap energy, $h\nu$ is photon energy, K is a constant, α is the absorption coefficient, and 'n' is an index that can take on different values depending on the interband transition mechanism [47]. Figure 3b exhibits the $(\alpha h\nu)^2$ versus energy graphs over which the bandgap values were plotted and found to be 3.61 eV, 3.59 eV, and 3.64 eV for SnO₂-1%, SnO₂-2%, and SnO₂-4% NPs, respectively. These values are similar to the 3.59 eV [48] and 3.6 eV [49] reported in the literature for SnO₂.

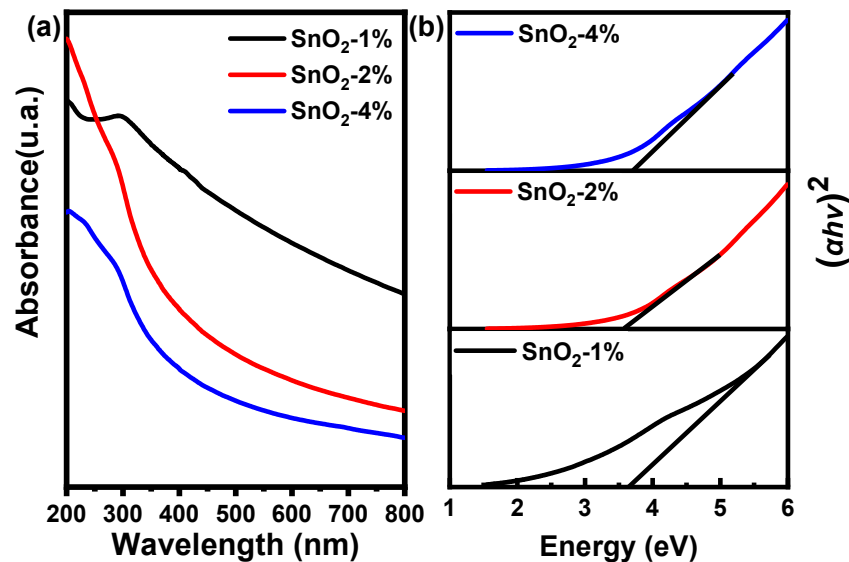


Figure 3. (a) UV-Vis spectra of SnO₂ NPs synthesized with *Tilia cordata* extract, and (b) Tauc model plot of SnO₂-1%, SnO₂-2%, and SnO₂-4% NPs synthesized with *Tilia cordata*, where the x-axis intercept was used to determine the bandgap.

3.4. Photoluminescence

Photoluminescence studies are important for investigating structural defects in NPs such as oxygen vacancies. Figure 4 shows the PL spectra for the SnO₂ NPs synthesized with different concentrations of *Tilia cordata* extract. The spectra were taken using a 350 nm excitation wavelength. SnO₂-1%, SnO₂-2%, and SnO₂-4% NPs present different emission bands centered at 360 nm, 379 nm for UV region and bands located at 448 nm, 466 nm, 480 nm, 490 nm, 509 nm, 525 nm and 559 nm, which correspond to the visible region. UV bands are related to the direct combination of electrons (e⁻) from the conduction band (CB) to holes (h⁺) in the valence band (VB) [50]. On the other hand, the green emission centered at 509 nm is attributed to the oxygen vacancies that help reduce the recombination rate of the electron–hole pairs, increasing their lifetime [51].

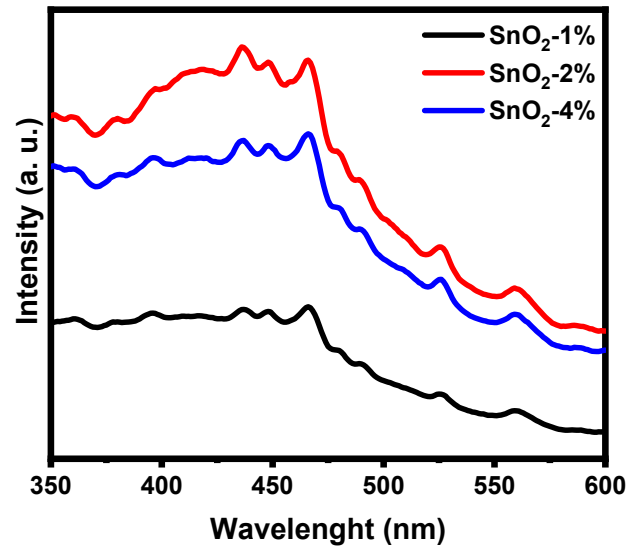


Figure 4. PL spectra of SnO₂ NPs synthesized with *Tilia cordata* extracts.

3.5. Surface Morphology

The SEM micrographs in Figure 5 show the surface morphology changes of the synthesized SnO₂ NPs with different *Tilia cordata* extract concentrations. Figure 5a depicts the SnO₂-1% NPs, which present a quasi-spherical morphology with agglomerations. Figure 5b illustrates a similar SnO₂-2% NP morphology to SnO₂-1%, but scattered and uniform in size with a few larger particles. Moreover, the SnO₂-4% NPs shown in Figure 5c present bumps supported on cluster-like particles and scattered, quasi-spherical particles; this could be due to the low nanoparticles nucleation caused by the high organic matter content [52,53], similar to those reported in the literature for SnO₂ NPs biosynthesis using natural extracts [30]. The EDX analyses (Table 1) elucidated three main elements, C, O, and Sn. Carbon can be associated with organic matter from *Tilia cordata* extracts, as shown by FTIR, because the amount of carbon increases as the concentration of the extract increases [54]. The occurrence of Sn and O elements confirms that the NPs obtained are SnO₂ [55].

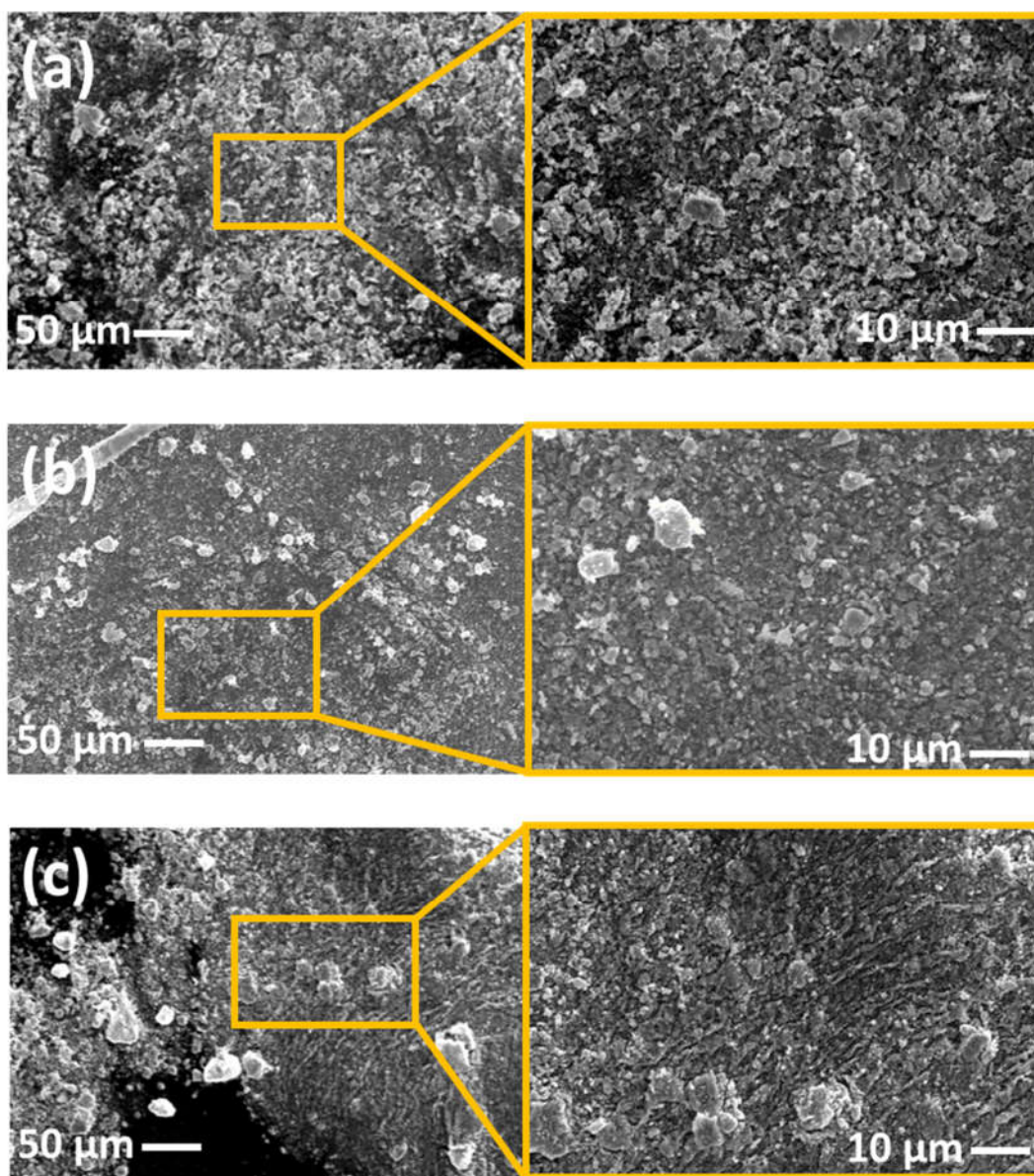


Figure 5. SEM micrographs of (a) SnO₂-1%, (b) SnO₂-2%, and (c) SnO₂-4% NPs.

Table 1. EDX of SnO₂ NPs synthesized with different concentrations of *Tilia cordata* extract.

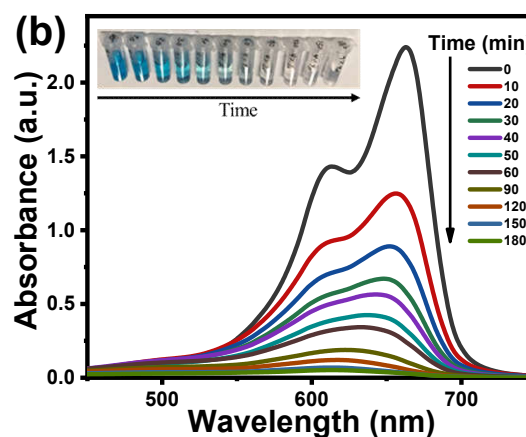
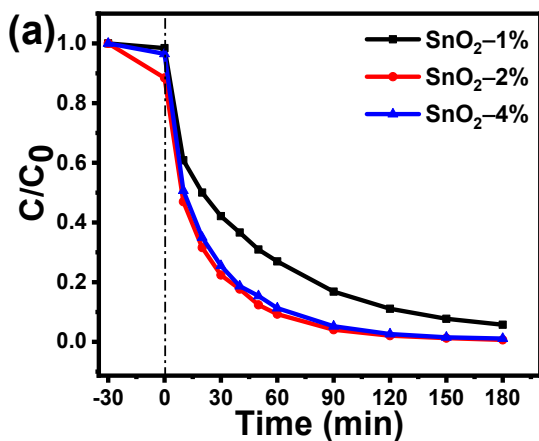
	% C	% O	% Sn
SnO ₂ -1%	8.96	26.24	64.8
SnO ₂ -2%	10.64	26.58	62.78
SnO ₂ -4%	18.21	28.96	52.83

3.6. Photocatalytic Activity

The photocatalytic activity of the SnO₂ NPs was evaluated for the MB dye photodegradation under UV and solar radiation. The results of MB degradation under UV radiation are shown in Figure 6a. It was observed that during the first hour, 73%, 90%, and 88% of dye was degraded by the SnO₂-1%, SnO₂-2%, and SnO₂-4% NPs, respectively, proving to

have a significant effect on dye degradation. Maximum MB degradation percentages of 94%, 99%, and 99% were reached at 180 min by the SnO₂-1%, SnO₂-2%, and SnO₂-4% samples, respectively. The difference in MB-degradation percentage can be attributed to the SnO₂ NPs size since the nanometric scale allows better dye, surface-adsorption, and provides higher availability of active sites to initiate degradation [56]. Additionally, the extract can function as a photosensitizer, thereby increasing the amount of extract increases photocatalytic activity [57]. Figure 6b shows the changes in the UV-Vis absorption spectrum of MB dye in the presence of SnO₂-2% NPs, where absorbance decreases over time, indicating concentration reduction. Additionally, the photograph in Figure 6b shows the photocatalysis process, which is visible as the color changes gradually. Correspondingly, Figure 6c shows the MB degradation percentages under solar radiation, where 48%, 68%, and 83.5% of MB were degraded after 180 min with SnO₂-1%, SnO₂-2%, and SnO₂-4% NPs, respectively, implying that under these study conditions there is a correlation between the amount of extract used in the synthesis of the NPs and the percentage of dye degradation.

These results confirm the successful synthesis of SnO₂ NPs using *Tilia cordata* extract and their excellent photocatalytic activity towards MB degradation. Table 2 mentions several SnO₂ NPs synthesis publications that evaluated MB photocatalysis in similar conditions. Certain stabilizing agents such as *Brassica oleracea* L. var. *botrytis* and *Jujube* extracts have similar effects on MB photocatalysis. However, the NPs synthesized with *Tilia cordata* transcend for their high efficiency, degrading up to 90% of the dye in just 60 min under UV radiation and 83.5% under solar radiation after 180 min.



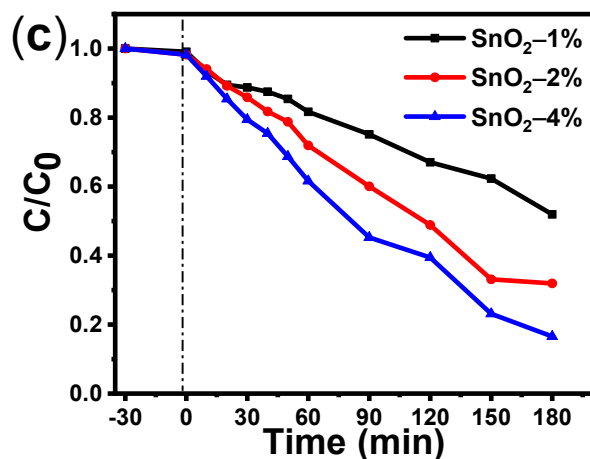


Figure 6. MB photocatalytic degradation (a) under UV radiation, (b) UV-Vis absorption spectra of the MB dye vs. time using SnO₂-2% NPs as photocatalysts, and (c) photocatalytic MB degradation under solar radiation.

Table 2. Comparison of MB photodegradation using SnO₂ NPs synthesized by different methods.

Method of Synthesis	Reducing/ Stabilizing Agent	Radiation	NPs Dose (mg)	Time (min)	Degradation (%)	Ref.
Plant extract	<i>Brassica oleracea L.</i> <i>var. botrytis</i>	UV	20	180	88.23–91.89	[58]
Plant extract	<i>Jujube</i>	Solar	8	300	90	[59]
Plant extract	<i>Cyphomandra</i> <i>betacea</i>	UV	25	70	>99	[60]
Plant extract	<i>Zea Maiz</i> activated carbon	Solar	20	120	71.92	[61]
Microwave	Arginine	Solar	10	240	96.4	[62]
Precipitation	H ₂ O ₂ , KOH	UV	4	180	79	[63]
Coprecipitation	Ammonia, surfactants	UV	100	120	53	[64]
Hydrothermal	NaOH, etOH	Solar	20, 40, 60	120	83, 97, 95	[65]
Plant extract	<i>Tilia cordata</i>	UV–Solar	50	60	90	This work

3.7. Degradation Mechanism

The dye degradation mechanism through photocatalysis using SnO₂ NPs is shown in Figure 7. The process is activated by the incidence of solar or UV radiation that promotes electrons from the valence band (VB) to the conduction band (CB), originating electron–hole pairs (e⁻/h⁺) in both [61]. The e⁻/h⁺ pairs can react directly with H₂O and O₂, generating highly reactive species such as hydrogen peroxide, hydroxyl radicals, and superoxide radicals. The radical species O₂• and OH• interact with dye molecules, degrading them to mineralization [66,67]. The MB degradation process (Figure 8) by photocatalysis with SnO₂ NPs can be set off by photogenerated holes as well as by OH• radicals, which attack the C–S=C functional groups of MB, generating sulfoxide groups (C–S(=O)–C). Then, the OH• radicals attack the sulfoxide group causing ring dissociation; the byproducts react to generate intermediate byproducts until the dye is degraded to mineralization, as reported by Bhattacharjee et al. [68].

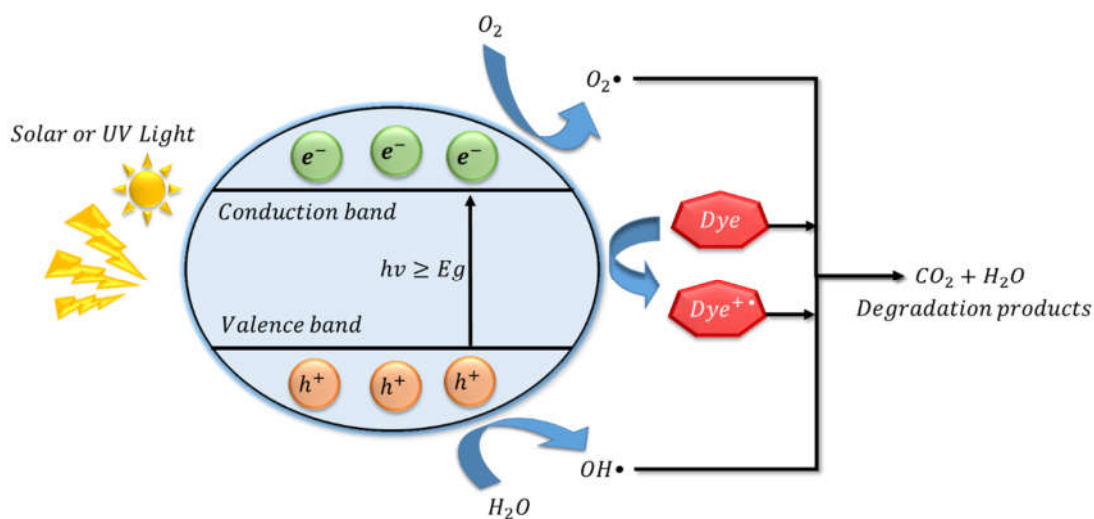


Figure 7. MB degradation mechanism with SnO₂ NPs synthesized utilizing *Tilia cordata* extract.

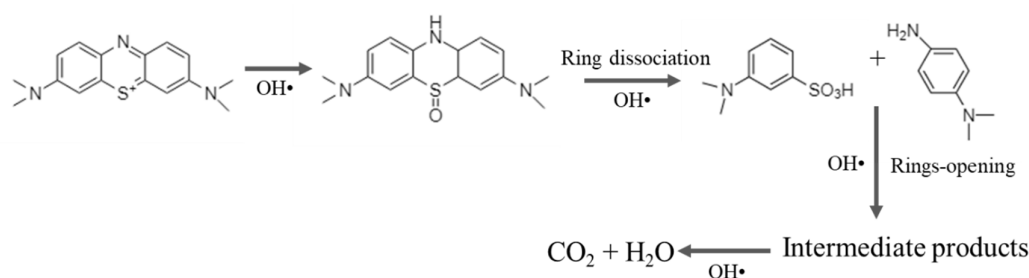


Figure 8. Proposed MB degradation mechanism through photocatalysis; adapted from [68].

4. Conclusions

In summary, SnO₂ NPs were successfully synthesized by a green and simple method, using *Tilia cordata* extract. The effects of extract concentration were evaluated, and it was determined that it had a significant influence on the nanoparticles' optical and morphological properties, as well as crystallite size and photocatalytic activity. The morphology analyses revealed that all SnO₂ NPs presented a quasi-spherical morphology and agglomerations, while the structural analyses of all synthesized materials revealed a rutile-type tetragonal crystalline structure, with crystallite sizes of 15.96 nm, 16.38 nm, and 21.51 nm for SnO₂-1%, SnO₂-2%, and SnO₂-4%, respectively, whereas the bandgap values remained at ~3.6 eV. The SnO₂ NPs presented excellent photocatalytic activity; UV radiation had a significant effect on the degradation of MB, resulting in 73%, 90%, and 88% degradation by SnO₂-1%, SnO₂-2%, and SnO₂-4% during the first hour. Moreover, the degradation percentages reached under solar radiation after 180 min were 48%, 68%, and 83.5%, with SnO₂-1%, SnO₂-2%, and SnO₂-4%, respectively. These studies presented similar and improved photocatalytic properties correspondingly to literature reports, demonstrating that *Tilia cordata*, used as a reducing agent, is a good candidate for the biosynthesis of semiconductor materials with application in the degradation of organic dyes by photocatalysis.

Author Contributions: E.Q.-G. investigation, methodology, formal analysis, writing-original draft. E.L.-M. investigation, methodology, formal analysis. R.V.Q.-R. conceptualization, formal analysis, writing-review & editing. H.E.G.-G. methodology, visualization. Y.A.B.-L. investigation, visualization. E.V.-V. investigation, visualization. F.A.-M. investigation, visualization. A.R.V.-N.

methodology, visualization P.A.L.M. conceptualization, investigation, writing-review & editing, supervision, validation. All authors have read and agreed to the published version of the manuscript.

Funding: This research received no external funding.

Institutional Review Board Statement: Not applicable.

Informed Consent Statement: Not applicable.

Data Availability Statement: Not applicable.

Acknowledgments: R.V. Quevedo-Robles acknowledgment CONACyT for postdoctoral scholarship.

Conflicts of Interest: The authors declare no conflict of interest.

References

1. Danish, M.S.S.; Estrella, L.L.; Alemaida, I.M.A.; Lisin, A.; Moiseev, N.; Ahmadi, M.; Nazari, M.; Wali, M.; Zaheb, H.; Senjyu, T. Photocatalytic Applications of Metal Oxides for Sustainable Environmental Remediation. *Metals* **2021**, *11*, 80. <https://doi.org/10.3390/met11010080>.
2. Routoula, E.; Patwardhan, S. v Degradation of Anthraquinone Dyes from Effluents: A Review Focusing on Enzymatic Dye Degradation with Industrial Potential. *Environ. Sci. Technol.* **2020**, *54*, 647–664.
3. Al-Tohamy, R.; Ali, S.S.; Li, F.; Okasha, K.M.; Mahmoud, Y.A.-G.; Elsamahy, T.; Jiao, H.; Fu, Y.; Sun, J. A critical review on the treatment of dye-containing wastewater: Ecotoxicological and health concerns of textile dyes and possible remediation approaches for environmental safety. *Ecotoxicol. Environ. Saf.* **2022**, *231*, 113160. <https://doi.org/10.1016/j.ecoenv.2021.113160>.
4. Topaç, F.O.; Dindar, E.; Uçaroğlu, S.; Başkaya, H.S. Effect of a sulfonated azo dye and sulfanilic acid on nitrogen transformation processes in soil. *J. Hazard. Mater.* **2009**, *170*, 1006–1013. <https://doi.org/10.1016/j.jhazmat.2009.05.080>.
5. Schneider, K.; Hafner, C.; Jäger, I. Mutagenicity of Textile Dye Products. *J. Appl. Toxicol. Int. J.* **2004**, *24*, 83–91.
6. Arshad, H.; Imran, M.; Ashraf, M. Toxic effects of Red-S3B dye on soil microbial activities, wheat yield, and their alleviation by pressmud application. *Ecotoxicol. Environ. Saf.* **2020**, *204*, 111030. <https://doi.org/10.1016/j.ecoenv.2020.111030>.
7. Kishor, R.; Bharagava, R.N.; Saxena, G. Industrial Wastewaters: The Major Sources of Dye Contamination in the Environment, Ecotoxicological Effects, and Bioremediation Approaches. In *Recent Advances in Environmental Management*; CRC Press: Boca Raton, FL, USA, 2018; pp. 1–25, ISBN 1351011251.
8. Zhou, Y.; Lu, J.; Zhou, Y.; Liu, Y. Recent Advances for Dyes Removal Using Novel Adsorbents: A Review. *Environmental Pollution* **2019**, *252*, 352–365.
9. Dotto, J.; Fagundes-Klen, M.R.; Veit, M.T.; Palácio, S.M.; Bergamasco, R. Performance of different coagulants in the coagulation/flocculation process of textile wastewater. *J. Clean. Prod.* **2018**, *208*, 656–665. <https://doi.org/10.1016/j.jclepro.2018.10.112>.
10. Le, T.M.H.; Nuisin, R.; Mongkolnavin, R.; Painmanakul, P.; Sairiam, S. Enhancing dye wastewater treatment efficiency in ozonation membrane contactors by chloro- and fluoro-organosilanes' functionality on hydrophobic PVDF membrane modification. *Sep. Purif. Technol.* **2022**, *288*, 120711. <https://doi.org/10.1016/j.seppur.2022.120711>.
11. Shoukat, R.; Khan, S.J.; Jamal, Y. Hybrid anaerobic-aerobic biological treatment for real textile wastewater. *J. Water Process Eng.* **2019**, *29*, 100804. <https://doi.org/10.1016/j.jwpe.2019.100804>.
12. Fujishima, A.; Honda, K. Electrochemical Photolysis of Water at a Semiconductor Electrode. *Nature* **1972**, *238*, 37–38. <https://doi.org/10.1038/238037a0>.
13. Saravanan, A.; Kumar, P.S.; Vo, D.-V.N.; Yaashikaa, P.R.; Karishma, S.; Jeevanantham, S.; Gayathri, B.; Bharathi, V.D. Photocatalysis for removal of environmental pollutants and fuel production: A review. *Environ. Chem. Lett.* **2020**, *19*, 441–463. <https://doi.org/10.1007/s10311-020-01077-8>.
14. Malato, S.; Maldonado, I.M.; Fernández-Ibáñez, P.; Oller, I.; Polo, I.; Sánchez-Moreno, R. Decontamination and Disinfection of Water by Solar Photocatalysis: The Pilot Plants of the Plataforma Solar de Almeria. *Mater Sci. Semicond. Process* **2016**, *42* (part 1), 15–23.
15. Enesca, A. The Influence of Photocatalytic Reactors Design and Operating Parameters on the Wastewater Organic Pollutants Removal—A Mini-Review. *Catalysts* **2021**, *11*, 556. <https://doi.org/10.3390/catal11050556>.
16. Youssef, Z.; Colombeau, L.; Yesmurzayeva, N.; Baros, F.; Vanderesse, R.; Hamieh, T.; Toufaily, J.; Frochot, C.; Roques-Carmes, T.; Acherar, S. Dye-sensitized nanoparticles for heterogeneous photocatalysis: Cases studies with TiO₂, ZnO, fullerene and graphene for water purification. *Dye. Pigment.* **2018**, *159*, 49–71. <https://doi.org/10.1016/j.dyepig.2018.06.002>.
17. El-Belely, E.F.; Farag, M.M.S.; Said, H.A.; Amin, A.S.; Azab, E.; Gobouri, A.A.; Fouda, A. Green Synthesis of Zinc Oxide Nanoparticles (ZnO-NPs) Using *Arthrospira platensis* (Class: Cyanophyceae) and Evaluation of their Biomedical Activities. *Nanomaterials* **2021**, *11*, 95. <https://doi.org/10.3390/nano11010095>.
18. Yousefi, S.R.; Alshamsi, H.A.; Amiri, O.; Salavati-Niasari, M. Synthesis, characterization and application of Co/Co₃O₄ nanocomposites as an effective photocatalyst for discoloration of organic dye contaminants in wastewater and antibacterial properties. *J. Mol. Liq.* **2021**, *337*, 116405. <https://doi.org/10.1016/j.molliq.2021.116405>.

19. Osman, N.S.; Sulaiman, S.N.; Muhamad, E.N.; Mukhair, H.; Tan, S.T.; Abdullah, A.H. Synthesis of an Ag₃PO₄/Nb₂O₅ Photocatalyst for the Degradation of Dye. *Catalysts* **2021**, *11*, 458.
20. Mallikarjunaswamy, C.; Pramila, S.; Nagaraju, G.; Ramu, R.; Ranganatha, V.L. Green Synthesis and Evaluation of Antiangiogenic, Photocatalytic, and Electrochemical Activities of BiVO₄ Nanoparticles. *J. Mater. Sci. Mater. Electron.* **2021**, *32*, 14028–14046.
21. Mahdi, M.A.; Yousefi, S.R.; Jasim, L.S.; Salavati-Niasari, M. Green Synthesis of DyBa₂Fe₃O₇. 988/DyFeO₃ Nanocomposites Using Almond Extract with Dual Eco-Friendly Applications: Photocatalytic and Antibacterial Activities. *Int. J. Hydrog. Energy* **2022**, *47*, 14319–14330.
22. Buniyamin, I.; Akhir, R.; Asli, N.A.; Khusaimi, Z.; Mahmood, M.R. Biosynthesis of SnO₂ nanoparticles by aqueous leaves extract of *Aquilaria malaccensis* (agarwood). *IOP Conf. Series: Mater. Sci. Eng.* **2021**, *1092*, 012070. <https://doi.org/10.1088/1757-899x/1092/1/012070>.
23. Maruthupandy, M.; Muneeswaran, T.; Chackaravarthi, G.; Vennila, T.; Anand, M.; Cho, W.-S.; Quero, F. Synthesis of chitosan/SnO₂ nanocomposites by chemical precipitation for enhanced visible light photocatalytic degradation efficiency of congo red and rhodamine-B dye molecules. *J. Photochem. Photobiol. A Chem.* **2022**, *430*, 113972. <https://doi.org/10.1016/j.jphotochem.2022.113972>.
24. Gomathi, E.; Jayapriya, M.; Arulmozhi, M. Environmental benign synthesis of tin oxide (SnO₂) nanoparticles using *Actinidia deliciosa* (Kiwi) peel extract with enhanced catalytic properties. *Inorg. Chem. Commun.* **2021**, *130*, 108670. <https://doi.org/10.1016/j.inoche.2021.108670>.
25. Luque, P.; Chinchillas-Chinchillas, M.; Nava, O.; Lugo-Medina, E.; Martínez-Rosas, M.; Carrillo-Castillo, A.; Vilchis-Nestor, A.; Madrigal-Muñoz, L.; Garrafa-Gálvez, H. Green synthesis of tin dioxide nanoparticles using *Camellia sinensis* and its application in photocatalytic degradation of textile dyes. *Optik* **2021**, *229*, 166259. <https://doi.org/10.1016/j.ijleo.2021.166259>.
26. Garrafa-Gálvez, H.; Nava, O.; Soto-Robles, C.; Vilchis-Nestor, A.; Castro-Beltrán, A.; Luque, P. Green synthesis of SnO₂ nanoparticle using *Lycopersicon esculentum* peel extract. *J. Mol. Struct.* **2019**, *1197*, 354–360. <https://doi.org/10.1016/j.molstruc.2019.07.052>.
27. Sagadevan, S.; Lett, J.A.; Fatimah, I.; Lokanathan, Y.; Léonard, E.; Oh, W.C.; Hossain, M.A.M.; Johan, M.R. Current Trends in the Green Syntheses of Tin Oxide Nanoparticles and Their Biomedical Applications. *Mater Res Express.* **2021**, *8*, 082001, doi:10.1088/2053-1591/ac187e.
28. Yadav, A.; Kon, K.; Kratošová, G.; Durán, N.; Ingle, A.P.; Rai, M. Fungi as an efficient mycosystem for the synthesis of metal nanoparticles: Progress and key aspects of research. *Biotechnol. Lett.* **2015**, *37*, 2099–2120. <https://doi.org/10.1007/s10529-015-1901-6>.
29. Al-Enazi, N.M.; Alwakeel, S.; Alhomaidi, E. Photocatalytic and biological activities of green synthesized SnO₂ nanoparticles using *Chlorella vulgaris*. *J. Appl. Microbiol.* **2022**, *00*, 1–11. <https://doi.org/10.1111/jam.15607>.
30. Gour, A.; Jain, N.K. Advances in green synthesis of nanoparticles. *Artif. Cells, Nanomedicine, Biotechnol.* **2019**, *47*, 844–851. <https://doi.org/10.1080/21691401.2019.1577878>.
31. Suresh, K.C.; Surendhiran, S.; Kumar, P.M.; Kumar, E.R.; Khadar, Y.A.S.; Balamurugan, A. Green synthesis of SnO₂ nanoparticles using *Delonix elata* leaf extract: Evaluation of its structural, optical, morphological and photocatalytic properties. *SN Appl. Sci.* **2020**, *2*, 1–13. <https://doi.org/10.1007/s42452-020-03534-z>.
32. Karthik, K.; Revathi, V.; Tatarchuk, T. Microwave-assisted green synthesis of SnO₂ nanoparticles and their optical and photocatalytic properties. *Mol. Cryst. Liq. Cryst.* **2018**, *671*, 17–23. <https://doi.org/10.1080/15421406.2018.1542080>.
33. Rathinabala, R.; Thamizselvi, R.; Padmanabhan, D.; Alshahateet, S.F.; Fatimah, I.; Sibhatu, A.K.; Weldegebrerial, G.K.; Razak, S.I.A.; Sagadevan, S. Sun light-assisted enhanced photocatalytic activity and cytotoxicity of green synthesized SnO₂ nanoparticles. *Inorg. Chem. Commun.* **2022**, *143*, 109783. <https://doi.org/10.1016/j.inoche.2022.109783>.
34. D'Ambrosio, U. *Tilia Platyphyllos y Tilia Cordata*; Pardo De Santayana, M., Morales, R., Tardío, J., Molina, M., Eds.; *Inventario*; Ministerio De Agricultura y Pesca, Alimentación y Medio Ambiente: Madrid, Spain, 2018.
35. Cittan, M.; Altuntaş, E.; Çelik, A. Evaluation of Antioxidant Capacities and Phenolic Profiles in *Tilia Cordata* Fruit Extracts: A Comparative Study to Determine the Efficiency of Traditional Hot Water Infusion Method. *Ind. Crops Prod.* **2018**, *122*, 553–558.
36. Saygi, K.O.; Cacan, E. Antioxidant and cytotoxic activities of silver nanoparticles synthesized using *Tilia cordata* flowers extract. *Mater. Today Commun.* **2021**, *27*, 102316. <https://doi.org/10.1016/j.mtcomm.2021.102316>.
37. Beevi, A.F.; Sreekala, G.; Beena, B. Synthesis, characterization and photocatalytic activity of SnO₂, ZnO nanoparticles against congo red: A comparative study. *Mater. Today Proc.* **2021**, *45*, 4045–4051. <https://doi.org/10.1016/j.matpr.2020.10.755>.
38. Van, K.N.; Huu, H.T.; Thi, V.N.N.; le Thi, T.L.; Truong, D.H.; Truong, T.T.; Dao, N.N.; Vo, V.; Vasseghian, Y. Facile Construction of S-Scheme SnO₂/g-C₃N₄ Photocatalyst for Improved Photoactivity. *Chemosphere* **2022**, *289*, 133120.
39. Mahakal, M.; Kutumbale, A.; Mehta, D.; Mehta, B.K. Green synthesis of zno nanoparticles from the methanolic extract of *embelia ribes* and their characterization by uv-visible, ftir, xrd and sem analysis. *International Journal of Pharmacy and Biological Sciences* **2018**, *8*, 402–409.
40. Ramesh, P.; Saravanana, K.; Manogar, P.; Johnson, J.; Vinoth, E.; Mayakannan, M. Green synthesis and characterization of biocompatible zinc oxide nanoparticles and evaluation of its antibacterial potential. *Sens. Bio-Sensing Res.* **2021**, *31*, 100399. <https://doi.org/10.1016/j.sbsr.2021.100399>.
41. Ben Soltan, W.; Ammar, S.; Olivier, C.; Toupance, T. Influence of zinc doping on the photocatalytic activity of nanocrystalline SnO₂ particles synthesized by the polyol method for enhanced degradation of organic dyes. *J. Alloy. Compd.* **2017**, *729*, 638–647. <https://doi.org/10.1016/j.jallcom.2017.09.155>.

42. Wan, W.; Li, Y.; Ren, X.; Zhao, Y.; Gao, F.; Zhao, H. 2D SnO₂ Nanosheets: Synthesis, Characterization, Structures, and Excellent Sensing Performance to Ethylene Glycol. *Nanomaterials* **2018**, *8*, 112. <https://doi.org/10.3390/nano8020112>.
43. Mustapha, F.; Jalil, A.; Mohamed, M.; Triwahyono, S.; Hassan, N.; Khusnun, N.; Hitam, C.; Rahman, A.F.A.; Firmanshah, L.; Zolkifli, A. New insight into self-modified surfaces with defect-rich rutile TiO₂ as a visible-light-driven photocatalyst. *J. Clean. Prod.* **2017**, *168*, 1150–1162. <https://doi.org/10.1016/j.jclepro.2017.09.095>.
44. Mahmood, H.; Khan, M.; Mohuddin, B.; Iqbal, T. Solution-phase growth of tin oxide (SnO₂) nanostructures: Structural, optical and photocatalytic properties. *Mater. Sci. Eng. B* **2020**, *258*, 114568. <https://doi.org/10.1016/j.mseb.2020.114568>.
45. Bhuvaneswari, K.; Nguyen, B.-S.; Nguyen, V.-H.; Nguyen, V.-Q.; Nguyen, Q.-H.; Palanisamy, G.; Sivashanmugan, K.; Pazhanivel, T. Enhanced photocatalytic activity of ethylenediamine-assisted tin oxide (SnO₂) nanorods for methylene blue dye degradation. *Mater. Lett.* **2020**, *276*, 128173. <https://doi.org/10.1016/j.matlet.2020.128173>.
46. Tauc, J. Optical properties and electronic structure of amorphous Ge and Si. *Mater. Res. Bull.* **1968**, *3*, 37–46. [https://doi.org/10.1016/0025-5408\(68\)90023-8](https://doi.org/10.1016/0025-5408(68)90023-8).
47. Yubero, F.; Jiménez, V.; Gonzalez-Eliphe, A. Optical properties and electronic transitions of SnO₂ thin films by reflection electron energy loss spectroscopy. *Surf. Sci.* **1998**, *400*, 116–126. [https://doi.org/10.1016/s0039-6028\(97\)00854-6](https://doi.org/10.1016/s0039-6028(97)00854-6).
48. Abdelkader, E.; Nadja, L.; Naceur, B.; Noureddine, B. SnO₂ foam grain-shaped nanoparticles: Synthesis, characterization and UVA light induced photocatalysis. *J. Alloy. Compd.* **2016**, *679*, 408–419. <https://doi.org/10.1016/j.jallcom.2016.04.016>.
49. Sadeghzadeh-Attar, A. Efficient photocatalytic degradation of methylene blue dye by SnO₂ nanotubes synthesized at different calcination temperatures. *Sol. Energy Mater. Sol. Cells* **2018**, *183*, 16–24. <https://doi.org/10.1016/j.solmat.2018.03.046>.
50. Wenderich, K.; Mul, G. Methods, Mechanism, and Applications of Photodeposition in Photocatalysis: A Review. *Chem. Rev.* **2016**, *116*, 14587–14619. <https://doi.org/10.1021/acs.chemrev.6b00327>.
51. Aly, B. Controlled optoelectronic properties and abrupt change in photosensitivity by suppressing density of oxygen vacancies in SnO₂ nanocrystalline thin films prepared at various spray-deposition temperatures. *Phys. Scr.* **2020**, *95*, 065807. <https://doi.org/10.1088/1402-4896/ab848f>.
52. Oskam, G. Metal oxide nanoparticles: Synthesis, characterization and application. *J. Sol-Gel Sci. Technol.* **2006**, *37*, 161–164. <https://doi.org/10.1007/s10971-005-6621-2>.
53. Jolivet, J.-P.; Henry, M.; Livage, J. *Metal Oxide Chemistry and Synthesis: From Solution to Solid State*; Wiley-Blackwell: New York, NY, USA, 2000; ISBN 0471970565.
54. Jadoun, S.; Arif, R.; Jangid, N.K.; Meena, R.K. Green synthesis of nanoparticles using plant extracts: A review. *Environ. Chem. Lett.* **2020**, *19*, 355–374. <https://doi.org/10.1007/s10311-020-01074-x>.
55. Yang, L.; Huang, J.; Liu, H.; Li, S.; Han, Y.; Qi, G.; Lv, M.; Shang, Y.; Ye, J. SnO₂-x/Sb₂O₃ composites synthesized by mechanical milling method with excellent photocatalytic properties for isopropyl alcohol oxidation. *J. Mater. Sci. Mater. Electron.* **2020**, *31*, 8564–8577. <https://doi.org/10.1007/s10854-020-03392-w>.
56. Nakibli, Y.; Mazal, Y.; Dubi, Y.; Wächtler, M.; Amirav, L. Size Matters: Cocatalyst Size Effect on Charge Transfer and Photocatalytic Activity. *Nano Lett.* **2017**, *18*, 357–364. <https://doi.org/10.1021/acs.nanolett.7b04210>.
57. Rodwihok, C.; Wongratanaphisan, D.; Ngo, Y.L.T.; Khandelwal, M.; Hur, S.H.; Chung, J.S. Effect of GO Additive in ZnO/rGO Nanocomposites with Enhanced Photosensitivity and Photocatalytic Activity. *Nanomaterials* **2019**, *9*, 1441. <https://doi.org/10.3390/nano9101441>.
58. Osuntokun, J.; Onwudiwe, D.C.; Ebenso, E.E. Biosynthesis and Photocatalytic Properties of SnO₂ Nanoparticles Prepared Using Aqueous Extract of Cauliflower. *J. Clust. Sci.* **2017**, *28*, 1883–1896. <https://doi.org/10.1007/s10876-017-1188-y>.
59. Honarmand, M.; Golmohammadi, M.; Naeimi, A. Biosynthesis of tin oxide (SnO₂) nanoparticles using jujube fruit for photocatalytic degradation of organic dyes. *Adv. Powder Technol.* **2019**, *30*, 1551–1557. <https://doi.org/10.1016/j.apt.2019.04.033>.
60. Elango, G.; Roopan, S.M. Efficacy of SnO₂ nanoparticles toward photocatalytic degradation of methylene blue dye. *J. Photochem. Photobiol. B: Biol.* **2016**, *155*, 34–38. <https://doi.org/10.1016/j.jphotobiol.2015.12.010>.
61. Ramamoorthy, M.; Ragupathy, S.; Sakthi, D.; Arun, V.; Kannadasan, N. Synthesis of SnO₂ loaded on corn cob activated carbon for enhancing the photodegradation of methylene blue under sunlight irradiation. *J. Environ. Chem. Eng.* **2020**, *8*, 104331. <https://doi.org/10.1016/j.jece.2020.104331>.
62. Bhattacharjee, A.; Ahmaruzzaman, M. A green and novel approach for the synthesis of SnO₂ nanoparticles and its exploitation as a catalyst in the degradation of methylene blue under solar radiation. *Mater. Lett.* **2015**, *145*, 74–78. <https://doi.org/10.1016/j.matlet.2015.01.029>.
63. Kim, S.P.; Choi, M.Y.; Choi, H.C. Photocatalytic activity of SnO₂ nanoparticles in methylene blue degradation. *Mater. Res. Bull.* **2016**, *74*, 85–89. <https://doi.org/10.1016/j.materresbull.2015.10.024>.
64. Sujatha, K.; Seethalakshmi, T.; Sudha, A.; Shanmugasundaram, O. Photocatalytic activity of pure, Zn doped and surfactants assisted Zn doped SnO₂ nanoparticles for degradation of cationic dye. *Nano-Structures Nano-Objects* **2019**, *18*, 100305. <https://doi.org/10.1016/j.nanoso.2019.100305>.
65. Sagadevan, S.; Lett, J.A.; Alshahateet, S.F.; Fatimah, I.; Weldegebrerial, G.K.; Le, M.-V.; Leonard, E.; Paiman, S.; Soga, T. Photocatalytic degradation of methylene blue dye under direct sunlight irradiation using SnO₂ nanoparticles. *Inorg. Chem. Commun.* **2022**, *141*, 109547. <https://doi.org/10.1016/j.inoche.2022.109547>.
66. Yang, X.; Wang, D. Photocatalysis: From Fundamental Principles to Materials and Applications. *ACS Appl. Energy Mater.* **2018**, *1*, 6657–6693. <https://doi.org/10.1021/acsaem.8b01345>.

67. Rosaline, D.R.; Suganthi, A.; Vinodhkumar, G.; Inbanathan, S.S.R.; Umar, A.; Ameen, S.; Akhtar, M.S.; LuizFoletto, E. Enhanced Sunlight-Driven Photocatalytic Activity of SnO₂-Sb₂O₃ Composite towards Emerging Contaminant Degradation in Water. *J Alloys Compd.* **2022**, *897*, 162935, doi:10.1016/j.jallcom.2021.162935.
68. Bhattacharjee, A.; M., A.; Th. Babita, D.; Jayashree, N. Photodegradation of Methyl Violet 6B and Methylene Blue Using Tin-Oxide Nanoparticles (Synthesized via a Green Route). *J. Photochem. Photobiol. A Chem.* **2016**, *325*, 116–124.